Hindawi
International Journal of Aerospace Engineering
Volume 2023, Article ID 8747790, 19 pages
https://doi.org/10.1155/2023/8747790

Research Article

Computational Optimal Impact Angle Control Guidance Laws Weighted by Arbitrary Functions

Qi Chen, Jinguang Shi, and Zhongyuan Wang

School of Energy and Power Engineering, Nanjing University of Science and Technology, Nanjing 210094, China

Correspondence should be addressed to Qi Chen; qichen@njust.edu.cn

Received 25 August 2022; Revised 7 October 2022; Accepted 8 November 2022; Published 5 January 2023

Academic Editor: Shaoming He

This paper presents a computational impact angle control guidance law based on the energy cost weighted by arbitrary functions in order to shape the acceleration command as desired. The optimal guidance problem is established in the impact angle frame and is solved by the Gauss orthogonal collocation method. The proposed guidance law is formulated from the generalized optimal control framework, thus a new guidance law that allows achieving a specific guidance goal can be easily obtained in the way of devising a proper weighting function (smooth, piecewise, nonsmooth, or even discontinuous). This property provides more degrees of freedom in the guidance law design to accomplish a specified guidance objective. A hardware experiment is conducted to evaluate the real-time computational capacity of the proposed computational guidance law. Illustrative examples with several types of weighting functions, including smooth, piecewise, nonsmooth, and discontinuous functions, are provided to demonstrate the advantages and capacity of the proposed guidance law.

1. Introduction

The main goal of designing a guidance law for an interception missile is to obtain a minimum miss distance with respect to a given target. However, to enhance the effect of kill probability, modern tactical missiles are expected not only to intercept the target but also to achieve a desired terminal impact angle [1–3]. Driven by these practical needs, intercept angle control guidance laws have been growing rapidly and become an important research topic.

In literature, a variety of guidance laws based on modern control theory have been devised to impose desired impact angle constraint, such as optimal guidance laws [4–8], sliding mode guidance laws [9–12], three-dimensional guidance laws [13–16], and L_2 gain-based guidance law [17]. It is known that the guidance laws based on optimal control theory can not only impose optimality in some particular performance indexes such as control effort and miss distance but also handle the terminal constraints easily. Therefore, a variety of efficient guidance laws have been widely reported using optimal control theory. Kim and Grider [18] proposed a suboptimal guidance law for reentry vehicles with a constraint on the body attitude angle at impact, where the guidance problem was formulated as a linear quadratic problem. By solving the energy minimization optimal control problem, Ryoo et al. [19] presented an optimal guidance law with impact angle constraints for both the lag free and the first-order missile systems. Therein, three methods of calculating the time-to-go using to construct the closed form of guidance command were also proposed. An optimal guidance law for impact angle control was developed in [20] for antitank and antiship missiles against maneuvering targets. To improve the survivability and effectiveness of missiles as much as possible, an optimal control based guidance law was proposed in [21] to control impact time and impact angle. By analyzing the dynamics of time-to-go error and introducing an impact time controller, an impact angle and time control guidance law is proposed along the corresponding time-to-go estimation. Based on flight model construction, Zhu et al. [22] presented a cruising guidance law with impact time and angle control, in which the time-to-go estimation is not required.

In the framework of optimal control-based guidance law design, the selection of the cost function is an important

issue because the response of state variables and the guidance performance are affected by the cost function. To shape the missile's trajectory and thus accomplish some specified guidance objectives, various weighted optimal guidance laws with impact angle constraint have been developed. In [23–25], a power of time-to-go function was adopted to weight the energy cost function, by which the robustness of the guidance law to external disturbances at the end of the homing phase was improved. For aerodynamically maneuvering ground-to-air missiles, an exponential function was employed for the weighting function of the energy cost in [26], where the penalty for late maneuvers was higher than for earlier ones, and thus the acceleration demand was distributed to compensate for the loss of aerodynamic maneuvering. Similarly, exponential weighting functions were suggested in [27] to shape guidance commands for surface-to-air missiles against high-speed incoming targets. An optimal guidance law providing some degree of freedom to prevent command saturation was devised by Lee et al. [28]. In this study, a Gaussian function was used as a weighting function to alleviate sensitivity with respect to initial heading error. Lee et al. [29] used sinusoidal functions to weight the energy performance index and proposed new guidance laws that generate a small acceleration at both the initial and final time for a stationary or slowly moving target. Xiong et al. [30] proposed an optimal impact angle control guidance law for a missile with time-varying velocity, where the impact angle costs and miss distance were weighted by the variants of hyperbolic tangent function while the energy cost was weighted by a power of time-to-go. This guidance law can produce a small acceleration command at the initial phase of the engagement.

In such previous works, for achieving the specified guidance purpose, particular weighting functions were introduced to shape the missile's trajectory or to distribute the acceleration demand during the engagement. Recently, generalized optimal impact angle guidance laws have been developed by using various approaches. In [31], the generalized formulations of optimal guidance laws were provided by solving optimal control problems with a generalized performance index, which showed that any positive function can be used as a weighting function. In [32], by taking into account the dynamic lag effect and the velocity variation, a more practical generalized optimal guidance law was proposed. In [33], the generalized guidance command is determined in a closed-loop feedback form by solving a linear quadratic optimal control problem with the energy consumption weighted by an arbitrary positive function. The above methods analytically studied the solution to the generalized optimal guidance problem, but mainly considered smooth weighting functions. If the weighting function can be devised arbitrarily (for instance, piecewise, nonsmooth, and discontinuous), the flexibility of guidance law design can be significantly increased. Consequently, this paper provides an alternative approach to solve optimal control problem with arbitrary weighting functions from a computational perspective. The main contributions of this paper are summarized as follows:

(1) A computational optimal guidance law that has the command shaping capacity is proposed by using the collocation method. The proposed guidance law is formulated from the generalized optimal control framework and a new guidance law that allows achieving a specific guidance goal can be easily obtained by devising a proper weighting function. In addition, the proposed guidance law can be easily extended to the dynamic lag system. The real-time computational capacity of the proposed approach is evaluated on a microprocessor

(2) The results presented are the first attempts in literature to introduce piecewise weighting functions. Owing to the elegant characteristics of piecewise functions, several guidance operational goals, such as providing small acceleration command at the initial time or at the final time or both at the initial time and final time, can be easily accomplished by using one single weighting function. However, in previous studies, to accomplish the aforementioned guidance goals several distinct weighting functions are required to designed specifically

(3) The proposed guidance has the capacity to easily tackle piecewise, nonsmooth, and discontinuous weighting functions, which can provide more degrees of freedom in the guidance law design to accomplish a specified guidance objective. Therefore, hybrid functions that consist of different forms of functions during different guidance phases can be considered for the weighting function of energy cost, which can take advantages of various weighting functions during the entire guidance process and thus hold the potential to significantly enhance the guidance performance

This paper is organized as follows. The engagement kinematics and problem formulation of optimal guidance law are described in Section 2. The derivation of optimal guidance law is presented in Section 3. Section 4 presents the hardware experiment and numerical simulation results. Conclusions are presented in Section 5.

2. Problem Formulation

Consider the engagement geometry for a stationary or a slowly moving target shown in Figure 1. In this geometry, M and T denote the missile and target, respectively. V_m, γ_m, and a_m denote the velocity, flight path angle, and normal acceleration of the missile, respectively. σ and γ_{f} represent the line-of-sight (LOS) angle and desired impact angle, respectively. The coordinate system OX_IY_I denotes the inertial reference frame, while the coordinate system TX_fY_f represents the impact angle frame. The frame TX_fY_f is fixed with the target and is rotated from OX_IY_I by the desired impact angle γ_{f}. $\bar{\gamma}_{\mathrm{m}}$ and $\bar{\sigma}$ denote the fight path angle of missile and LOS angle in the impact angle frame $TX_{\mathrm{f}}Y_{\mathrm{f}}$ and are expressed as

$$\begin{cases} \bar{\gamma}_{\mathrm{m}} = \gamma_{\mathrm{m}} - \gamma_{\mathrm{f}} \\ \bar{\sigma} = \sigma - \gamma_{\mathrm{f}} \end{cases}. \tag{1}$$

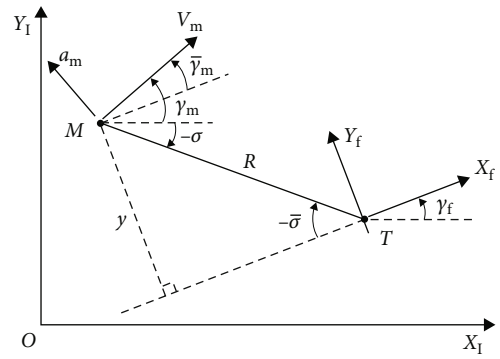

Figure 1: Engagement geometry.

It's seen from Equation (1) that $\bar{\gamma}_m$ can be regarded as the impact angle error. From Figure 1, the equations of motion for the engagement in impact angle frame TX_fY_f are given by.

$$\begin{cases} \dot{y}(t) = V_m(t)\sin\bar{\gamma}_m(t) \\ \dot{\bar{\gamma}}_m(t) = a_m(t)/V_m(t) \end{cases}, \tag{2}$$

where y represents the lateral distance perpendicular to the desired impact direction. Under the assumption that V_m is constant and $\bar{\gamma}_m$ is small, Equation (2) can be linearized as

$$\begin{cases} \dot{y}(t) = V_m(t)\bar{\gamma}_m(t) \\ \dot{\bar{\gamma}}_m(t) = a_m(t)/V_m(t) \end{cases}. \tag{3}$$

From Equation (3), the linearized engagement kinematics can be rewritten in a compact form as follows

$$\begin{cases} \boldsymbol{x}(t) = \boldsymbol{F}\boldsymbol{x}(t) + \boldsymbol{G}u(t) \\ \boldsymbol{x}(0) = \boldsymbol{x}_0 \end{cases}, \tag{4}$$

where

$$x \triangleq [y \quad \bar{\gamma}_m]^T, u \triangleq a_m F \triangleq \begin{bmatrix} 0 & V_m \\ 0 & 0 \end{bmatrix}, G = \begin{bmatrix} 0 \\ 1 \end{bmatrix}. \tag{5}$$

Note that the linearized kinematics (4) has been widely implemented to devise guidance laws with various constraints in many literatures [19, 24, 28, 29, 31, 32].

It can be seen from Figure 1 that if the missile velocity vector coincides with the axis TX_f, namely, $y = 0$ and $\bar{\gamma}\_m = 0$, then the impact angle interception will be guaranteed. Therefore, the terminal constraint for an interception and impact angle control are given by

$$\begin{cases} y(t_f) = 0 \\ \bar{\gamma}_m(t_f) = 0 \end{cases}, \tag{6}$$

where t_f denotes the final time of engagement. Now, consider the following finite-time optimal control problem: determine the control $u(t)$ that minimizes the cost function

Table 1: Conditions for nonlinear simulations.

Parameter	Value
Missile initial position, $(X_m(0), Y_m(0))$	(1000 m, 5000 m)
Target position, $(X_t(0), Y_t(0))$	(6000 m, 0 m)
Missile velocity, V_m	300 m/s
Initial flight path angle, $\gamma_m(0)$	-45°, -20°, 20°, 45°
Desired impact angle, γ_f	-70°, -90°

$$J = \frac{1}{2}\boldsymbol{x}^{\mathrm{T}}(t_{\mathrm{f}})\boldsymbol{S}_{\mathrm{f}}\boldsymbol{x}(t_{\mathrm{f}}) + \frac{1}{2}\int_{t_0}^{t_{\mathrm{f}}}\frac{u^2(\tau)}{S(\tau)}d\tau, \tag{7}$$

subject to Equation (4).

Here, t_0 is the initial time of engagement, $\boldsymbol{S}_f$ is a positive definite matrix and is used to control the terminal states of the missile, $S(t)$ is a weighting function. Note that, to guarantee the impact angle interception, the value of the matrix $\boldsymbol{S}_f$ should be selected as large as possible.

3. Derivation of Optimal Guidance Law

3.1. Optimal Solution Using the Gauss Orthogonal Collocation Method. In this section, the Gauss orthogonal collocation method is taken to solve the finite-time optimal control problem as shown in Equation (7). The Hamiltonian function of the optimal control problem is

$$H = \frac{1}{2}\frac{u^2(t)}{S(t)} + \boldsymbol{\lambda}(t)^{\mathrm{T}}[\boldsymbol{F}\boldsymbol{x}(t) + \boldsymbol{G}u(t)], \tag{8}$$

where $\boldsymbol{\lambda}(t)$ denotes the costate and satisfies the following adjoint equation

$$\dot{\lambda}(t) = -\frac{\partial H}{\partial x(t)} = -F^T\lambda(t), \tag{9}$$

with the transversality condition

$$\boldsymbol{\lambda}(t_{\mathrm{f}}) = \boldsymbol{S}_{\mathrm{f}}\boldsymbol{x}(t_{\mathrm{f}}). \tag{10}$$

From the minimum principle, it is necessary that

$$\frac{\partial H}{\partial u(t)} = 0, \tag{11}$$

which yields the following optimal control

$$u^*(t) = -\frac{1}{S(t)^{-1}}\boldsymbol{G}^{\mathrm{T}}\boldsymbol{\lambda}(t). \tag{12}$$

Substituting Equation (12) into Equation (4), and combining with the adjoint Equation (9) yields the following two-point boundary-value problem (TPBVP)

$$\begin{cases} \dot{x}(t) = \dfrac{\partial H}{\partial \lambda(t)} = Fx(t) - G\dfrac{1}{S(t)^{-1}}G^T\lambda(t), & x(t_0) = x_0 \\ \dot{\lambda}(t) = -\dfrac{\partial H}{\partial x(t)} = -F^T\lambda(t), & \lambda(t_f) = S_f x(t_f) \end{cases}. \tag{13}$$

To implement the Gauss orthogonal collocation method, the time interval $t \in [t_0, t_f]$ in Equation (13) should be transformed to $\tau \in [-1, 1]$. By using the following affine transformation

$$\tau = \frac{2}{t_f - t_0}t - \frac{t_f + t_0}{t_f - t_0}. \tag{14}$$

Equation (13) can be transformed into

$$\begin{cases} \dot{x}(\tau) = \dfrac{t_f - t_0}{2}\left[Fx(\tau) - G\dfrac{1}{S(\tau)^{-1}}G^T\lambda(\tau)\right], & x(-1) = x_0 \\ \dot{\lambda}(\tau) = -\dfrac{t_f - t_0}{2}F^T\lambda(\tau), & \lambda(1) = S_f x(1) \end{cases}. \tag{15}$$

The Gauss orthogonal collocation method to solve the optimal control problem Equation (7) is to discretize and transcribe the two-point boundary-value problem into a set of algebraic equations by approximating the state and costate trajectories via interpolating polynomials. The state $\boldsymbol{x}(\tau)$ is approximated using a basis of $N + 1$ Lagrange interpolating polynomials,

$$\boldsymbol{x}(\tau) \approx \mathbf{X}(\tau) = \boldsymbol{x}(-1)L_0(\tau) + \sum_{k=1}^{N}\boldsymbol{x}(\tau_k)L_k(\tau), \tag{16}$$

where $L_k(\tau)(k = 0, \cdots, N)$ are defined as

$$L_k(\tau) = \prod_{i=0, i\neq k}^{N}\frac{\tau - \tau_i}{\tau_k - \tau_i}. \tag{17}$$

Note that the boundary point, -1, and the N Gauss points, τ_k, are used to construct the approximation of $\boldsymbol{x}(\tau)$. Differentiating the expression in Equation (16) gives

$$\dot{x}(\tau) \approx \dot{X}(\tau) = x(-1)\dot{L}_0(\tau) + \sum_{k=1}^{N}x(\tau_k)\dot{L}_k(\tau). \tag{18}$$

Because the initial value of $\boldsymbol{\lambda}(\tau)$ is unknown, whereas the terminal value of $\boldsymbol{\lambda}(\tau)$ is known and given by

$$\lambda(1) = \boldsymbol{S}_f\boldsymbol{x}(1). \tag{19}$$

Therefore, the N Gauss points, τ_k, and the boundary point, 1, are used to construct the approximation of $\boldsymbol{\lambda}(\tau)$ as follows

$$\boldsymbol{\lambda}(\tau) \approx \boldsymbol{\Lambda}(\tau) = \sum_{k=1}^{N}\boldsymbol{\lambda}(\tau_k)L_k^*(\tau) + \boldsymbol{\lambda}(1)L_{N+1}^*(\tau), \tag{20}$$

where $L_k^*(\tau)$ $(k = 1, \cdots, N + 1)$ are defined as

$$L_k^*(\tau) = \prod_{i=1, i\neq k}^{N+1}\frac{\tau - \tau_i}{\tau_k - \tau_i}. \tag{21}$$

Differentiating the expression in Equation (20) gives

$$\dot{\lambda}(\tau) \approx \dot{\Lambda}(\tau) = \sum_{k=1}^{N}\lambda(\tau_k)\dot{L}_k^*(\tau) + \lambda(1)\dot{L}_{N+1}^*(\tau). \tag{22}$$

The terminal value of the state, $\boldsymbol{x}(1)$, can be obtained in terms $\boldsymbol{x}(\tau_k)$ and $\boldsymbol{\lambda}(\tau_k)$ via the Gauss quadrature [34].

$$\boldsymbol{x}(1) = \boldsymbol{x}(-1) + \frac{t_\mathrm{f} - t_0}{2}\sum_{k=1}^{N}w_k\left[\boldsymbol{F}x(\tau_k) - \boldsymbol{G}\frac{1}{S(\tau)^{-1}}\boldsymbol{G}^\mathrm{T}\lambda(\tau_k)\right], \tag{23}$$

where w_k are the Gaussian weights and can be calculated offline. Substituting Equation (23) into Equation (19) yields

$$\lambda(1) = \boldsymbol{S}_\mathrm{f}\boldsymbol{x}(-1) + \boldsymbol{S}_\mathrm{f}\frac{t_\mathrm{f} - t_0}{2}\sum_{k=1}^{N}w_k\left[\boldsymbol{F}x(\tau_k) - \boldsymbol{G}\frac{1}{S(\tau)^{-1}}\boldsymbol{G}^\mathrm{T}\lambda(\tau_k)\right]. \tag{24}$$

Denote $\bar{D}_i = \dot{L}_0(\tau_i)$, $D_{ik} = \dot{L}_k(\tau_i)$, $\bar{D}_i^* = \dot{L}_{N+1}^*(\tau)$, and $D_{ik}^* = \dot{L}_k^*(\tau)$; Substituting Equation (24) into Equation (22) and including Equation (18) yields

$$\begin{cases} \bar{D}_i^*\boldsymbol{S}_\mathrm{f}\boldsymbol{x}_0 + \bar{D}_i^*\boldsymbol{S}_\mathrm{f}\dfrac{t_\mathrm{f} - t_0}{2}\displaystyle\sum_{k=1}^{N}w_k\left[\boldsymbol{F}x_k - \boldsymbol{G}\frac{1}{S_k^{-1}}\boldsymbol{G}^\mathrm{T}\lambda_k\right] + \sum_{k=1}^{N}\lambda_k D_{ik}^* = -\dfrac{t_\mathrm{f} - t_0}{2}\boldsymbol{F}^\mathrm{T}\lambda_i \\ \boldsymbol{x}_0\bar{D}_i + \displaystyle\sum_{k=1}^{N}\boldsymbol{x}_k D_{ik} = \dfrac{t_\mathrm{f} - t_0}{2}\left[\boldsymbol{F}\boldsymbol{x}_i - \boldsymbol{G}\frac{1}{S_i^{-1}}\boldsymbol{G}^\mathrm{T}\lambda_i\right] \end{cases}, \tag{25}$$

where $i = 1, \cdots, N, \boldsymbol{x}k = \boldsymbol{x}(\tau_k), \boldsymbol{\lambda}_k = \boldsymbol{\lambda}(\tau_k), Sk = S(\tau_k)$ and $k = 1, \cdots, N$.

As proven in [35], the differential approximation matrices, $\boldsymbol{D} \in \mathbb{R}^{N\times N}$, $\bar{\boldsymbol{D}} \in \mathbb{R}^N$, $\boldsymbol{D}^* \in \mathbb{R}^{N\times N}$, and $\bar{\boldsymbol{D}}^* \in \mathbb{R}^N$ have the following relationships:

$$\begin{cases} \bar{D}_i = -\displaystyle\sum_{k=1}^{N}D_{ik}, \\ D_{ik}^* = -\dfrac{w_k}{w_i}D_{ki}, \\ \bar{D}_i^* = -\displaystyle\sum_{k=1}^{N}D_{ik}^*. \end{cases} \tag{26}$$

The elements of the differential approximation matrix

D can be determined offline by

$$D_{ik} = \dot{L}_i(\tau_k) = \sum_{l=0}^{N} \frac{\prod_{j=0,j\neq i,l}^{N}(\tau_k - \tau_j)}{\prod_{j=0,j\neq i}^{N}(\tau_i - \tau_j)}. \tag{27}$$

Consequently, the elements of the matrices $\bar{D}$, D^*, and $\bar{D}^*$ can be obtained offline via Equation (26).

Denote $\tilde{\Lambda} = [\lambda_1^T, \lambda_2^T, \cdots, \lambda_N^T]^T \in \mathbb{R}^{nN}$, $\tilde{X} = [x_1^T, x_2^T, \cdots, x_N^T]^T \in \mathbb{R}^{nN}$. Equation (25) can be rewritten as

$$\begin{cases} \tilde{\bar{D}}^* x_0 + \tilde{D}_+^* \tilde{\Lambda} + \tilde{A}\tilde{X} = 0 \\ \tilde{\bar{D}} x_0 + \tilde{D}_- \tilde{X} + \tilde{B}\tilde{\Lambda} = 0 \end{cases}, \tag{28}$$

where

$$\tilde{\bar{D}}^* = \begin{bmatrix} \bar{D}_1^* S_f \\ \vdots \\ \bar{D}_N^* S_f \end{bmatrix} \in \mathbb{R}^{nN\times n}, \tag{29}$$

$$\tilde{\bar{D}} = \begin{bmatrix} \bar{D}_1 I_n \\ \vdots \\ \bar{D}_N I_n \end{bmatrix} \in \mathbb{R}^{nN\times N}, \tag{30}$$

$$\tilde{D}_+^* = \begin{bmatrix} D_{11}^* I_n & D_{12}^* I_n & \cdots & D_{1N}^* I_n \\ D_{21}^* I_n & D_{22}^* I_n & \cdots & D_{2N}^* I_n \\ \vdots & \vdots & \ddots & \vdots \\ D_{N1}^* I_n & D_{N2}^* I_n & \cdots & D_{NN}^* I_n \end{bmatrix} - \frac{t_f - t_0}{2} \begin{bmatrix} \bar{D}_1^* S_f w_1 G \frac{1}{S_1^{-1}} G^T - F^T & \bar{D}_1^* S_f w_2 G \frac{1}{S_2^{-1}} G^T & \cdots & \bar{D}_1^* S_f w_N G \frac{1}{S_N^{-1}} G^T \\ \bar{D}_2^* S_f w_1 G \frac{1}{S_1^{-1}} G^T & \bar{D}_2^* S_f w_2 G \frac{1}{S_2^{-1}} G^T - F^T & \cdots & \bar{D}_2^* S_f w_N G \frac{1}{S_N^{-1}} G^T \\ \vdots & \vdots & \ddots & \vdots \\ \bar{D}_N^* S_f w_1 G \frac{1}{S_1^{-1}} G^T & \bar{D}_N^* S_f w_2 G \frac{1}{S_2^{-1}} G^T & \cdots & \bar{D}_N^* S_f w_N G \frac{1}{S_N^{-1}} G^T - F^T \end{bmatrix} \in \mathbb{R}^{nN\times nN}, \tag{31}$$

$$\tilde{D}_- = \begin{bmatrix} D_{11} I_n & D_{12} I_n & \cdots & D_{1N} I_n \\ D_{21} I_n & D_{22} I_n & \cdots & D_{2N} I_n \\ \vdots & \vdots & \ddots & \vdots \\ D_{N1} I_n & D_{N2} I_n & \cdots & D_{NN} I_n \end{bmatrix} - \frac{t_f - t_0}{2} \begin{bmatrix} F & 0_n & \cdots & 0_n \\ 0_n & F & \cdots & 0_n \\ \vdots & \vdots & \ddots & \vdots \\ 0_n & 0_n & \cdots & F \end{bmatrix} \in \mathbb{R}^{nN\times nN}, \tag{32}$$

$$\tilde{A} = \frac{t_f - t_0}{2} \begin{bmatrix} \bar{D}_1^* S_f w_1 F & \bar{D}_1^* S_f w_2 F & \cdots & \bar{D}_1^* S_f w_N F \\ \bar{D}_2^* S_f w_1 F & \bar{D}_2^* S_f w_2 F & \cdots & \bar{D}_2^* S_f w_N F \\ \vdots & \vdots & \ddots & \vdots \\ \bar{D}_N^* S_f w_1 F & \bar{D}_N^* S_f w_2 F & \cdots & \bar{D}_N^* S_f w_N F \end{bmatrix} \in \mathbb{R}^{nN\times nN}, \tag{33}$$

$$\tilde{B} = \frac{t_f - t_0}{2} \begin{bmatrix} G \frac{1}{S_1^{-1}} G^T & 0_n & \cdots & 0_n \\ 0_n & G \frac{1}{S_2^{-1}} G^T & \cdots & 0_n \\ \vdots & \vdots & \ddots & \vdots \\ 0_n & 0_n & \cdots & G \frac{1}{S_N^{-1}} G^T \end{bmatrix} \in \mathbb{R}^{nN\times nN}, \tag{34}$$

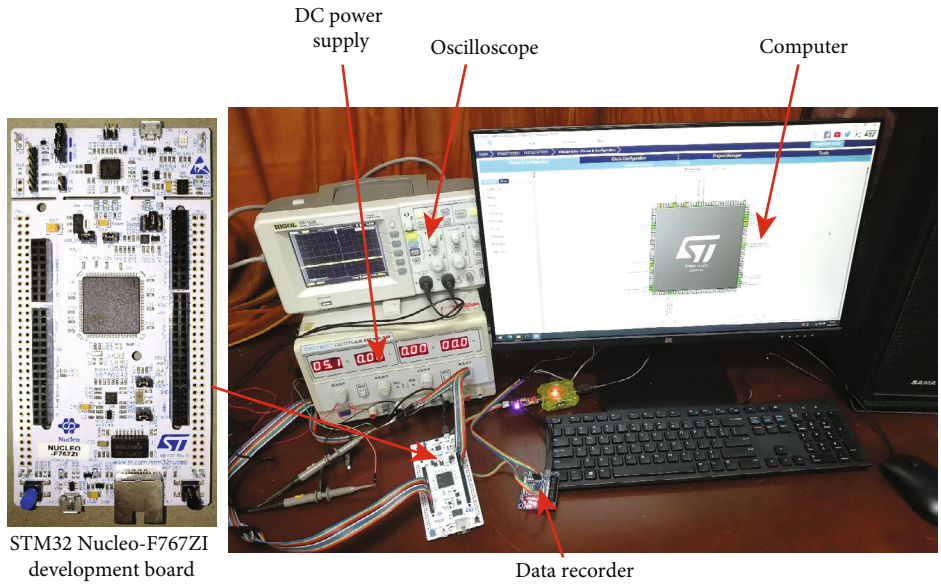

Figure 2: Hardware experiment setup.

Table 2: Computation time of the proposed guidance law.

C/C++ compiler optimization	FPU: VFPv5 single precision	Computation time (ms)		
		$N = 5$	$N = 10$	$N = 15$
High level with speed mode	Turn ON	1	6	15
None	Turn ON	3	10	21

and $\mathbf{0}_n$ is an $n \times n$ zero matrix, $\boldsymbol{I}_n$ is an $n \times n$ identity matrix. By denoting $\bar{D}_{aug} = \begin{bmatrix} \widetilde{\bar{D}}^* \\ \widetilde{\bar{D}} \end{bmatrix} \in \mathbb{R}^{2nN \times n}$ and $D_{aug} = \begin{bmatrix} \tilde{D}_+^* & \tilde{A} \\ \tilde{B} & \tilde{D}_- \end{bmatrix} \in \mathbb{R}^{2nN \times 2nN}$, Equation (28) can be expressed into the following compact form

$$\bar{D}_{\text{aug}} x_0 + D_{\text{aug}} \begin{bmatrix} \tilde{\Lambda} \\ \tilde{X} \end{bmatrix} = 0. \tag{35}$$

Solving for $\tilde{\Lambda}$ and $\tilde{X}$ in Equation (35) gives the solution to the two-point boundary-value problem (15) as

$$\begin{bmatrix} \tilde{\Lambda} \\ \tilde{X} \end{bmatrix} = -D_{\text{aug}}^{-1} \bar{D}_{\text{aug}} x_0. \tag{36}$$

From (36) the costate at the Gauss points can be directly determined from the initial state value $\boldsymbol{x}_0$. However, the Gauss points do not contain the boundary points, therefore, Equation (36) cannot provide the initial value of the costate, $\boldsymbol{\lambda}(-1)$. Because the terminal value of the costate, $\boldsymbol{\lambda}(1)$, is given in (24), therefore, $\boldsymbol{\lambda}(-1)$ can be calculated via the following Gauss quadrature [34].

$$\boldsymbol{\lambda}(-1) = \boldsymbol{\lambda}(1) - \frac{t_f - t_0}{2} \sum_{k=1}^{N} w_k \boldsymbol{F}^{\mathrm{T}} \boldsymbol{\lambda}_k. \tag{37}$$

According to Equations (12), (36), and (37), the optimal control at the boundary points as well as the Gauss points is obtained as

$$u_i^* = -\frac{1}{S_i^{-1}} \boldsymbol{G}^{\mathrm{T}} \boldsymbol{\lambda}_i \quad (i = 0, \cdots, N+1). \tag{38}$$

It is very important to note that the preceding derivation does not impose any constraint on $S(t)$ and the form of the equations are identical for $\boldsymbol{F}$, $\boldsymbol{G}$, and $S(t)$, indicating that the proposed method can easily and directly handle different and complex weighting functions without any modification. This property makes the guidance law design very flexible to accomplish the specified objective. In other words, arbitrary positive function can be used as a weighting function, thus the penalty for maneuvers can be adjusted accordingly by tuning the shape of the weighting function in order to achieve some specific guidance objective. In addition, it should be also noted that in our method, the optimal control is obtained without any explicit integration or construction of transition matrices, but only by solving algebraic equations.

3.2. Guidance Law Implementation. Note that the optimal solution obtained in Section 3.1 is open-loop for the

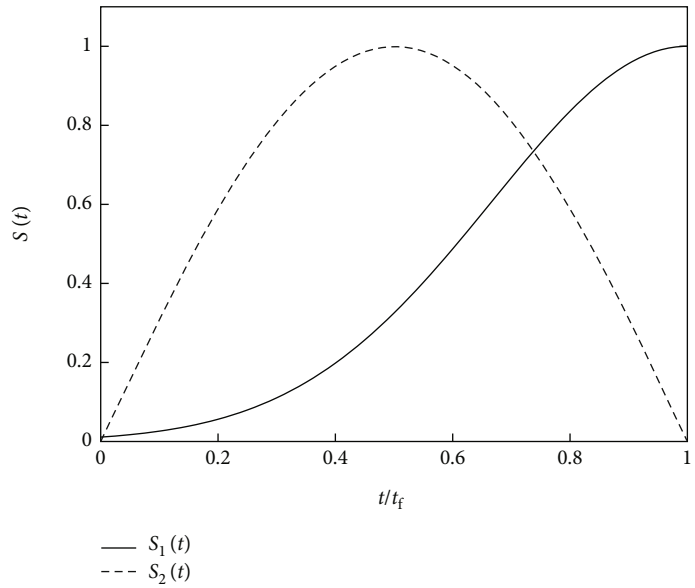

FIGURE 3: Profiles of the weighting function $S_1(t)$ and $S_2(t)$.

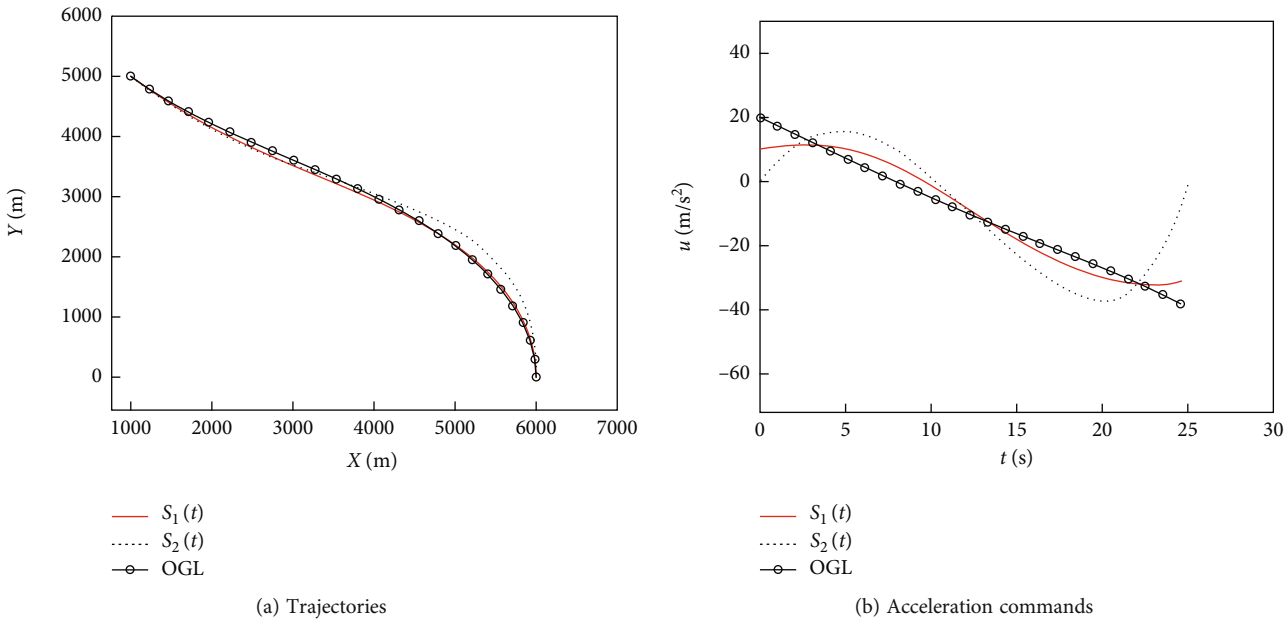

(a) Trajectories

(b) Acceleration commands

FIGURE 4: The comparison results of different weighting functions for $\gamma_m(0) = -45^\circ$, $\gamma_f = -90^\circ$.

guidance problem. To obtain the closed-loop solution, the receding-horizon technique is implemented. The receding-horizon length is chosen as the time-to-go (i.e., the time remaining to interception, and denoted as t_{go}), which is approximated by $t_{go} = R/V_m$. Consequently, the final time of engagement can be expressed as $t_f = t_0 + t_{go}$. The procedure for implementing the proposed guidance law with impact angle constraint can be summarized as follows.

(1) Initial number of the Gauss points, N, and set $t_0 = 0$

(2) Solve the sequence of TPBVP

(a) Calculate the time-to-go, t_{go}

(b) Calculate the matrices $\bar{D}_{aug}$ and $\bar{D}_{aug}$, and solve Equation (36).

(c) Update the control u_i $(i = 0, \cdots, N)$ using the solution from step 2b and Equation (38).

(3) Apply the control input at the current time at the first discretization point, u_0, to the missile's dynamics and update the missile's states at the next time

(4) Repeat steps 2-3 until intercepting the target

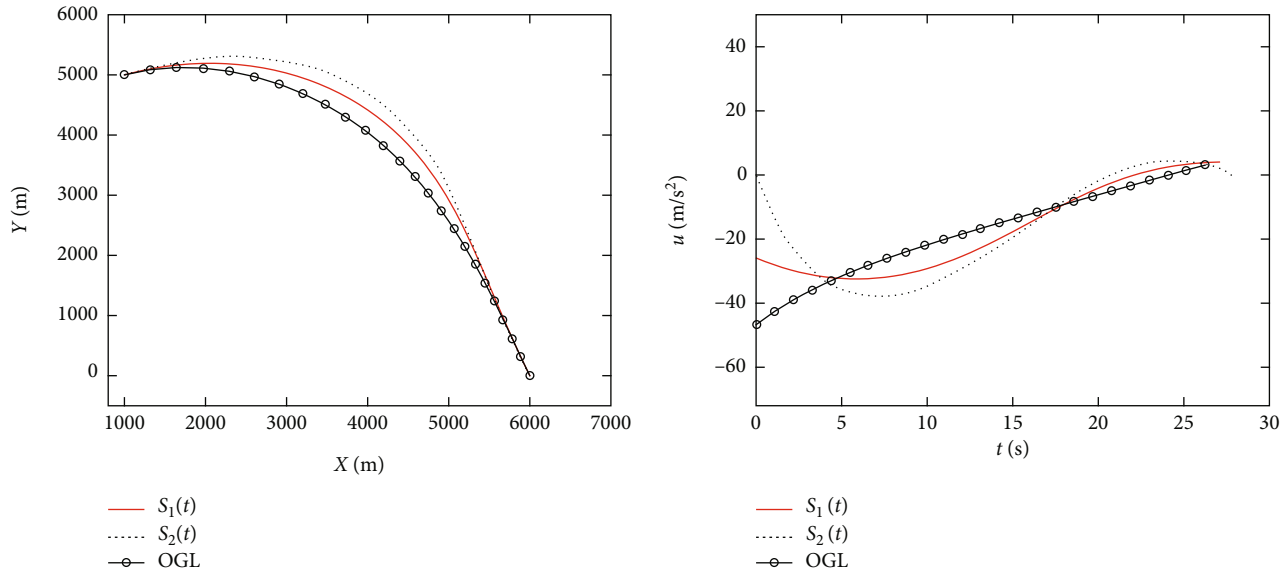

(a) Trajectories (b) Acceleration commands

Figure 5: The comparison results of different weighting functions for $\gamma_m(0) = 20\circ$, $\gamma_f = -70\circ$.

Table 3: Different parameters for $S_3(t)$.

Weighting function	Parameter of the sigmoid function based weighting function					
	A_1	B_1	A_2	B_2	w	t_1
$S_3^{(1)}(t)$	1.0	-1.0	1.0	-1.0	t_f/2.0	t_f/4.0
$S_3^{(2)}(t)$	0.0	1.0	0.0	1.0	t_f/2.0	t_f/4.0
$S_3^{(3)}(t)$	0.0	1.0	1.0	-1.0	t_f/6.0	t_f/5.0

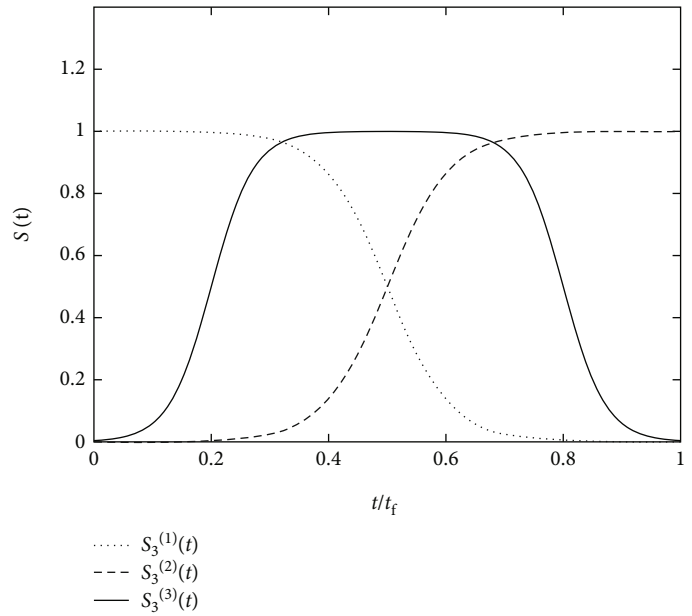

Figure 6: Profiles of the weighting function $S_3(t)$ with different designed parameters.

For complex weighting functions, the proposed method can easily obtain the optimal control via solving a set of algebraic equations and does not require any explicit propagation techniques (e.g. the backward sweep method). In addition, the derivation of the proposed guidance law does not rely on the concrete form of the weighting function, such

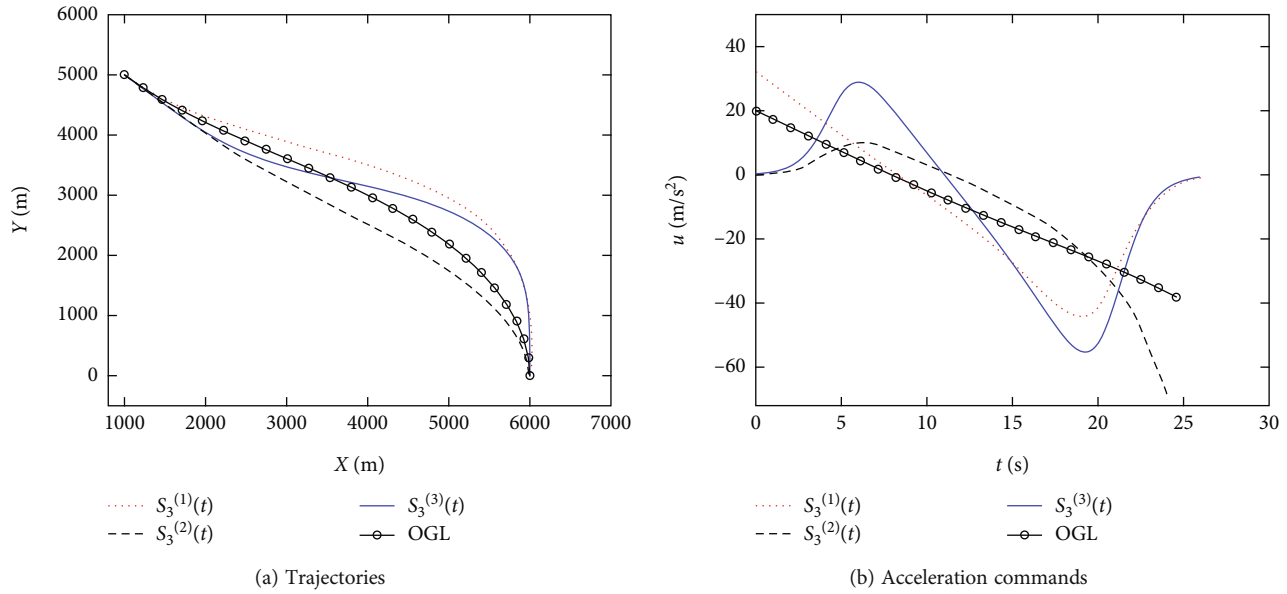

(a) Trajectories (b) Acceleration commands

Figure 7: The comparison results of different weighting functions for $\gamma_m(0) = -45\circ$, $\gamma_f = -90\circ$.

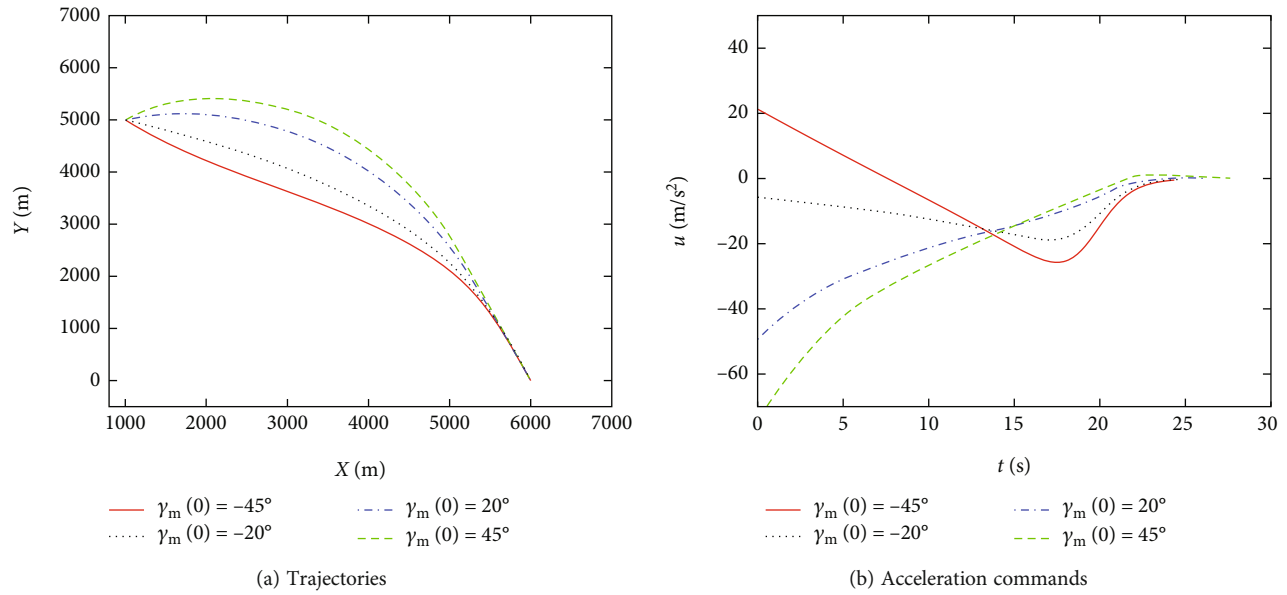

(a) Trajectories (b) Acceleration commands

Figure 8: The comparison results for various initial flight path angles with the weighting function $S_3^{(1)}(t)$.

that arbitrary positive function can be used as a weighting function. We will show later that complex weighting functions (smooth, piecewise, nonsmooth, and even discontinuous) can be easily employed in the proposed guidance law.

4. Hardware Experiment and Simulation Results

In this section, we will first evaluate the real-time computational capacity of the proposed guidance law, and then demonstrate its guidance performance under various weighting functions. The homing conditions for the simulations are given in Table 1.

4.1. Evaluation of Real-Time Computational Capacity. To assess the time-consuming property and the real-time computational capacity of the proposed guidance law, a hardware experimental platform based on the ARM Cortex-M7 processor is addressed in this section. The guidance law is performed on a STM32 Nucleo-F767ZI development board. The hardware experimental platform is shown in Figure 2. The microcontroller (STM32F767ZIT6U) used in the development board is based on the high-performance ARM Cortex-M7 32-bit RISC core operating at up to 216 MHz frequency, and features a floating-point unit (FPU) which supports ARM double-precision and single-precision processing instructions. To implement the guidance law on the hardware platform, the STM32Cube MX software is used to

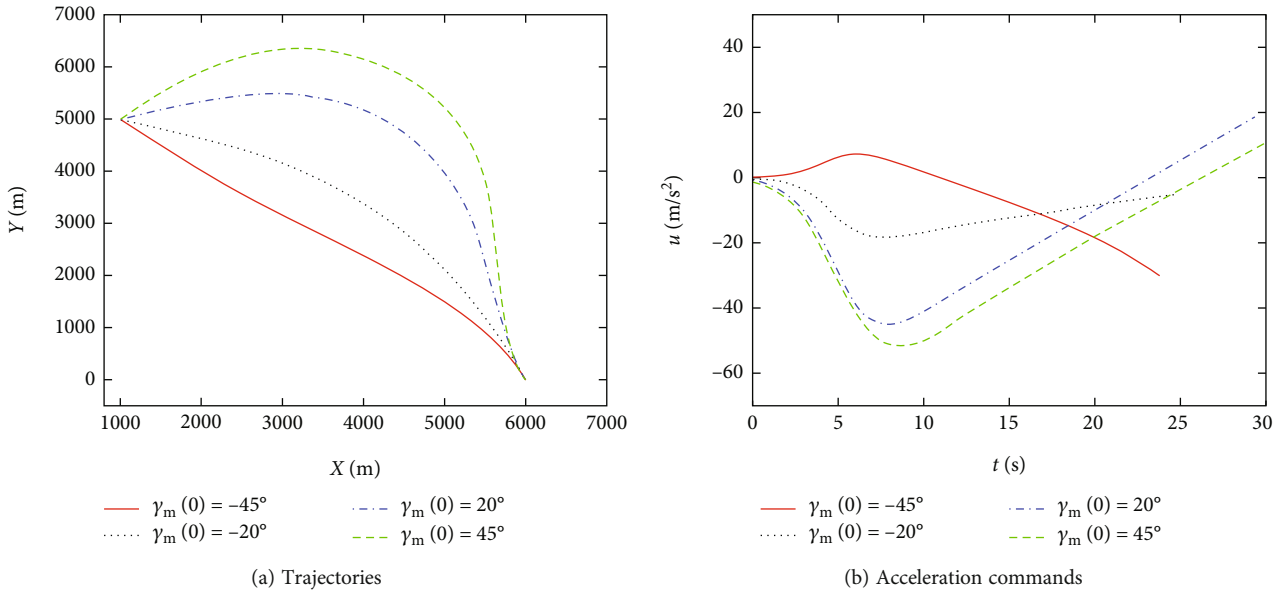

(a) Trajectories (b) Acceleration commands

FIGURE 9: The comparison results for various initial flight path angles with the weighting function $S_3^{(2)}(t)$.

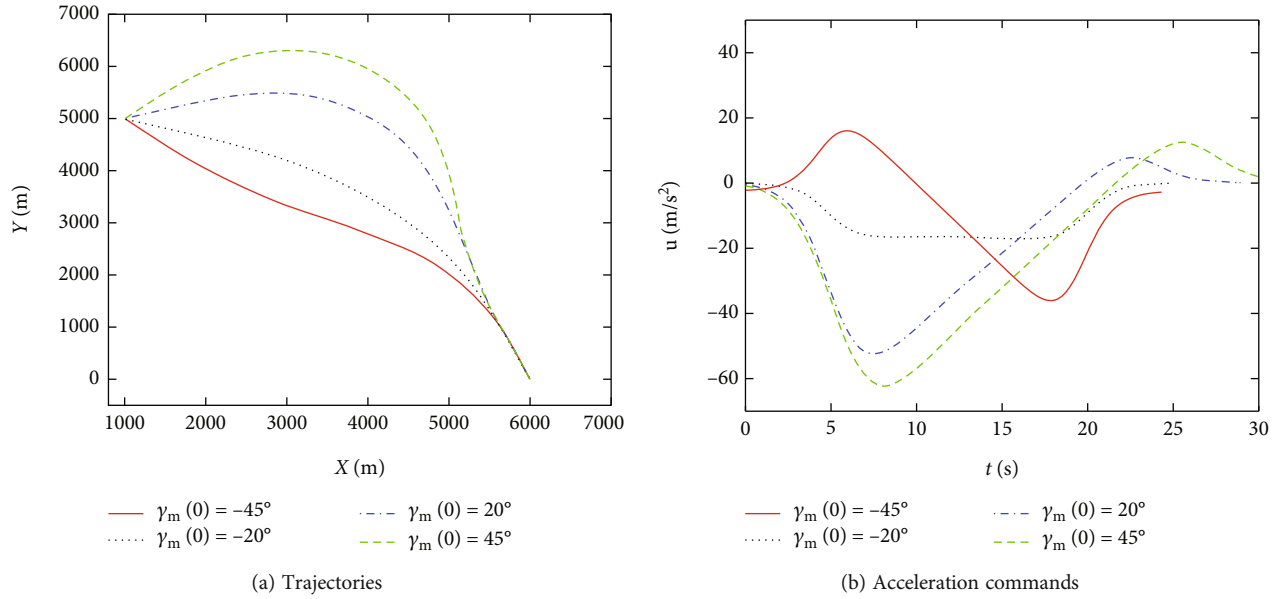

(a) Trajectories (b) Acceleration commands

FIGURE 10: The comparison results for various initial flight path angles with the weighting function $S_3^{(3)}(t)$.

generate the HAL-based embedded project of IAR compiler. All the matrix operations needed in the guidance law are carried out using the corresponding C functions provided by CMSIS DSP library, which is a built-in suite of common signal processing functions.

In the test, the compiler's code optimization of IAR is turned on and off, respectively, while the mode of single-precision FPU is turned on all the time. Table 2 summarizes the computation time of the proposed guidance law in one computation loop. It is seen that the computation time increases as the discretization point increases. The compiler optimization for the embedded code is helpful to reduce the computation time. By turning on the compiler optimization mode of IAR and selecting a proper number of discretization points, the computational time can be reduced to a satisfactory level, which means the proposed guidance law is computationally viable for onboard implementation. In addition, it is expected that the computation time will be further reduced by using other high performance processors (for instance, DSP and FPGA).

4.2. Performance of the Proposed Guidance Law. In this subsection, numerical examples are performed to illustrate the performance of the proposed guidance law. The initial conditions for the following simulation scenarios are listed in Table 1. In these simulations, five different types of

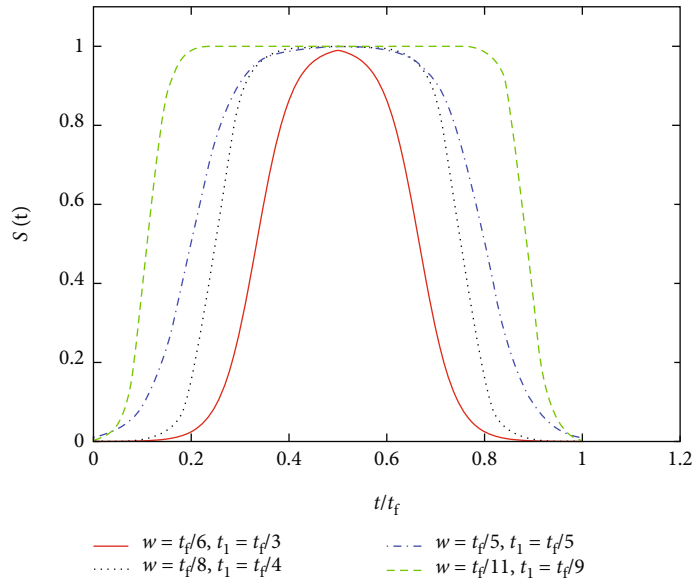

FIGURE 11: Profiles of the weighting function $S_3^{(3)}(t)$ with different values of w and t_1.

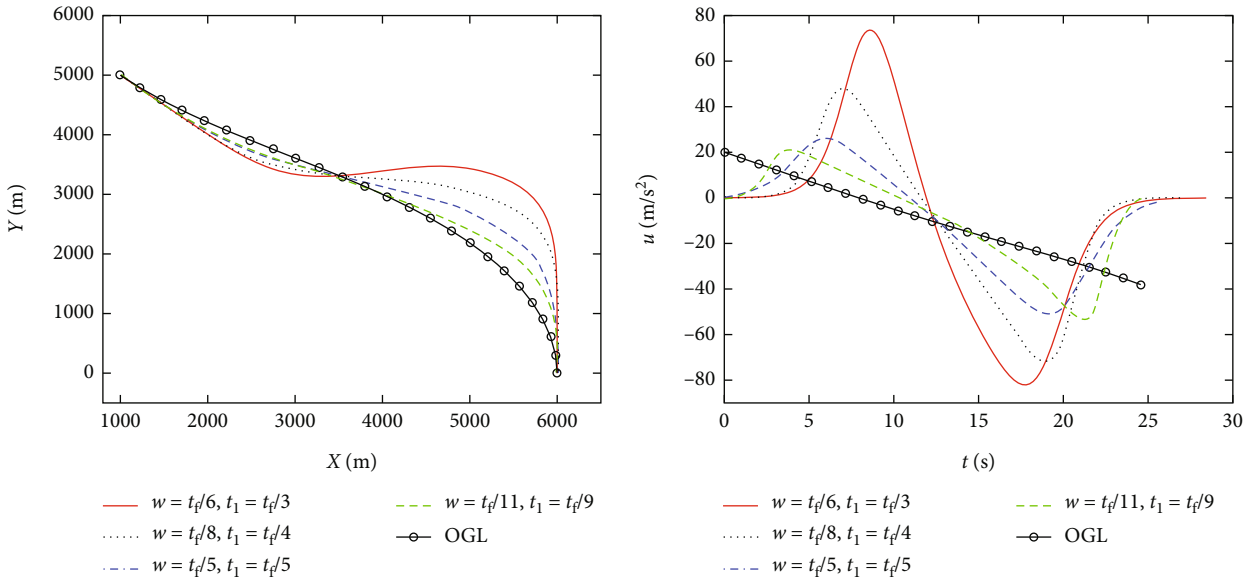

(a) Trajectories

(b) Acceleration commands

FIGURE 12: The comparison results of weighting functions $S_3^{(3)}(t)$ with different values of w and t_1.

weighting functions, including continuous, piecewise, nonsmooth, and discontinuous functions, are employed to demonstrate the capacity and the performance of the proposed guidance law. The number of the Gauss points, N, is selected to be 15. $\boldsymbol{S}_f$ is chosen to be $[1 \times 10^4, 1 \times 10^4]^T$.

4.2.1. Case 1: Gaussian and Sinusoidal Weighting Functions. In this case, we take the Gaussian weighting function and the sinusoidal weighting function, which were originally presented in [28, 29], as an example to demonstrate that the proposed guidance law has the capacity to tackle existing weighting functions easily. The Gaussian weighting function $S_1(t)$ and the sinusoidal weighting function $S_2(t)$ are as follows:

$$S_1(t) = \frac{1}{e^{\left(t-t_f/2\right)^2/2\tau_\sigma^2}}, \tag{39}$$

$$S_2(t) = \sin\left[\frac{\pi}{t_f}\left(t_f - t\right)\right]. \tag{40}$$

$S_1(t)$ is adopted to shape the specific guidance command: introducing a small acceleration at the initial time. While $S_2(t)$ is adopted to shape the specific guidance

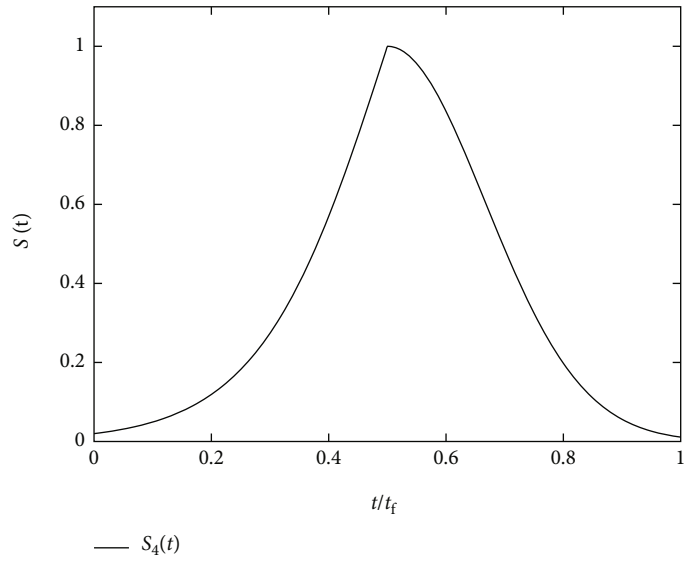

Figure 13: Profile of the weighting function $S_4(t)$.

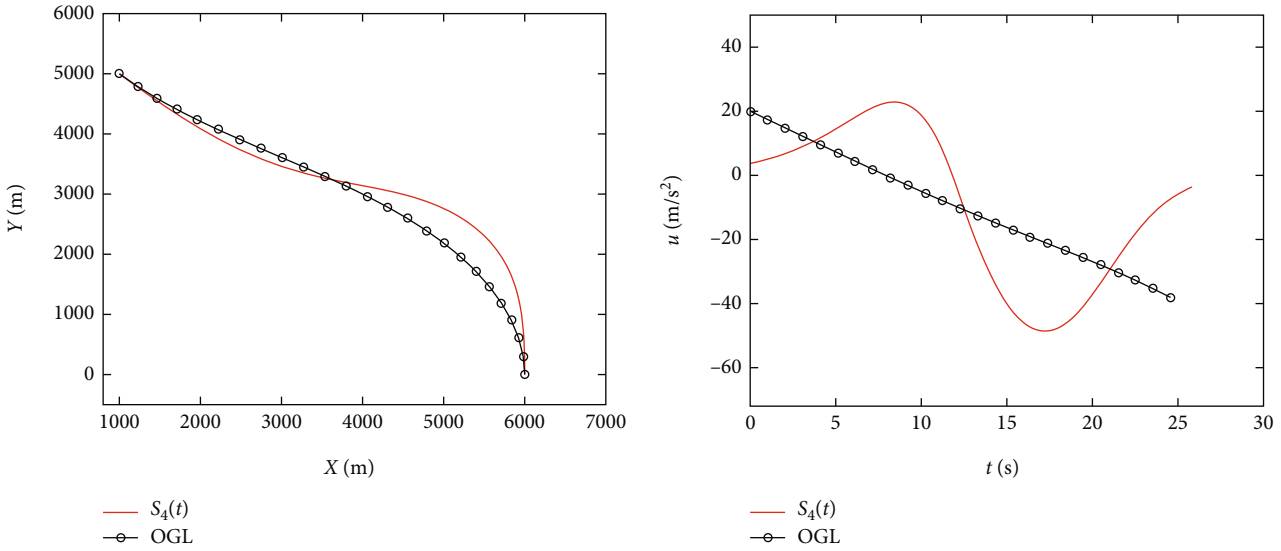

(a) Trajectories

(b) Acceleration commands

Figure 14: The comparison results of different weighting functions for $\gamma_m(0) = -45^\circ$, $\gamma_f = -90^\circ$.

command: introducing a small acceleration at the initial and final time. In this case, we set τ_σ as $t_f/3.0$ for $S_1(t)$. The profiles of $S_1(t)$ and $S_2(t)$ are shown in Figure 3. As can be seen, the weighting profile of $S_1(t)$ approaches zero values at the initial time, while the weighting profile of $S_2(t)$ approaches zero values at the initial time and the final time. Detailed descriptions for $S_1(t)$ and $S_2(t)$ can be referred to [28, 29].

For comparison purposes, the impact angle control optimal guidance law called OGL that is presented in [19] is also applied in the simulation. Figures 4 and 5 show the intercept trajectories and guidance commands for various weighting functions. The proposed approach can easily tackle the Gaussian weighting function and the sinusoidal weighting function, and successfully provide zero miss distance with the desired impact angle for all cases as shown in Figures 4(a) and 5(a). The guidance commands are clearly shaped by different weighting functions as shown in Figures 4(b) and 5(b). Specifically, the command of OGL approaches a nonzero value at both the initial and final time. This profile may result in an abrupt change of guidance command at the initial time and a performance degradation at the final time under the presences of external disturbances. However, the Gaussian weighting $S_1(t)$ generates a small acceleration command at the initial time compared with OGL, while the sinusoidal weighting function $S_2(t)$ always generates zero initial command and also converges to a zero value as the missile approaches a target. These

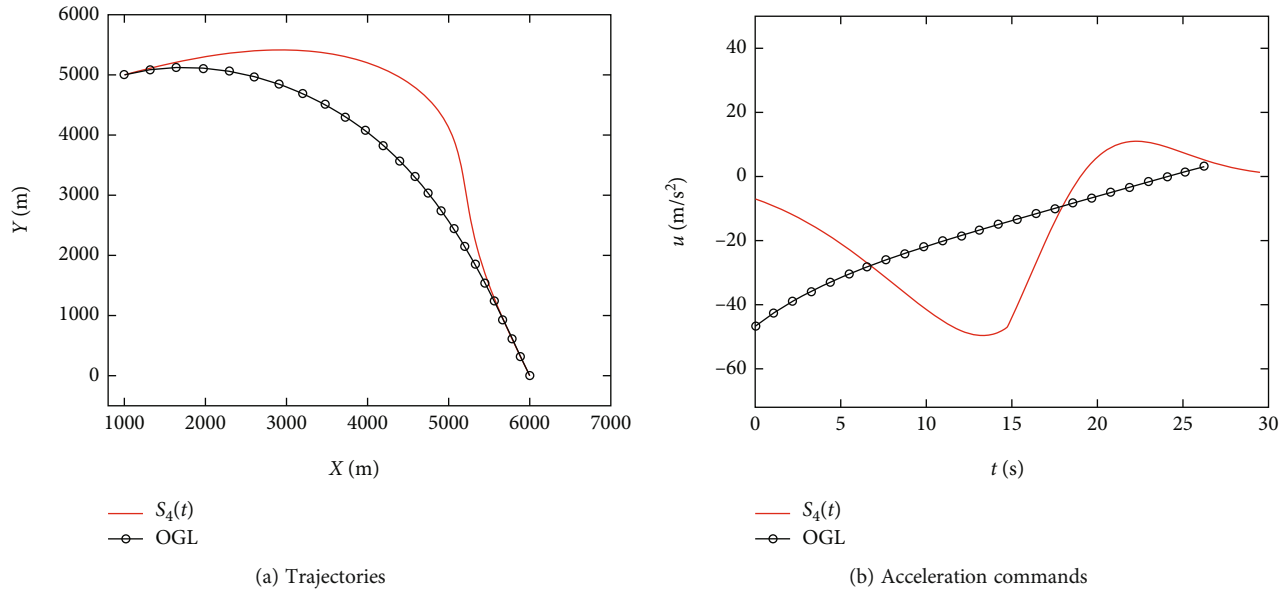

(a) Trajectories (b) Acceleration commands

Figure 15: The comparison results of different weighting functions for $\gamma_m(0) = 20\circ$, $\gamma_f = -70\circ$.

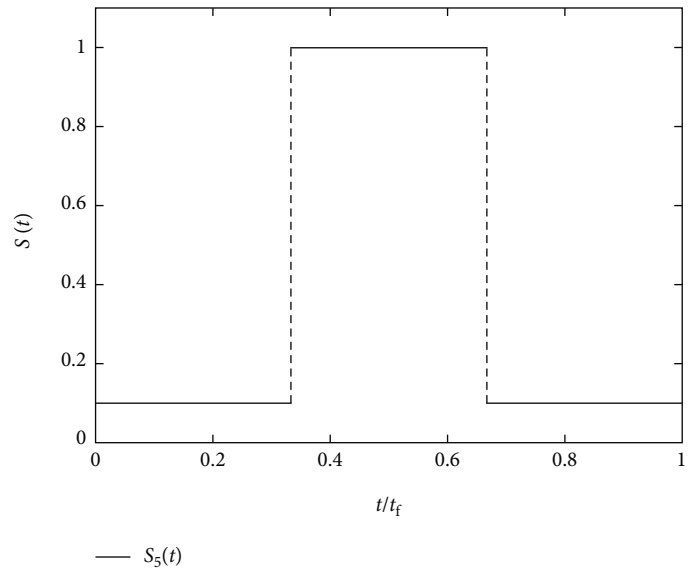

Figure 16: Profile of the weighting function $S_5(t)$.

properties can improve the guidance command, alleviating sensitivity with respect to initial heading error, or improving the lethality of the warhead and guaranteeing operational margin to cope with external disturbances in the vicinity of target. The above results are consistent with the analyses in [28, 29]. Since the proposed guidance law is formulated from the generalized optimal control framework, the existing weighting functions (e.g., Gaussian and sinusoidal) can be easily incorporated into the proposed approach for achieving various guidance goals.

4.2.2. Case 2: Sigmoid-Based Weighting Function. In this case, we constructed a new kind of piecewise weighting function based on the sigmoid function as

$$S_3(t) = \begin{cases} A_1 + \dfrac{B_1}{1 + e^{-(4.6/w)(t-t_1)}} & 0 \le t \le \dfrac{t_f}{2} \\ A_2 + \dfrac{B_2}{1 + e^{-(4.6/w)(t-t_f+t_1)}} & \dfrac{t_f}{2} < t \le t_f \end{cases}, \tag{41}$$

where A_1, B_1, A_2, B_2, w, and t_1 are designed parameters. According to selections of the designed parameters (i.e., A_1, B_1, A_2, B_2, w, and t_1), various weighting profiles can be generated. Table 3 provides three kind of combinations of A_1, B_1, A_2, B_2, w, and t_1, and the corresponding profiles of $S_3(t)$ are shown in Figure 6.

As seen in Figure 6, $S_3(t)$ can be utilized to shape the specific guidance command: providing small acceleration command at the initial time ($S_3^{(1)}(t)$) or at the final time

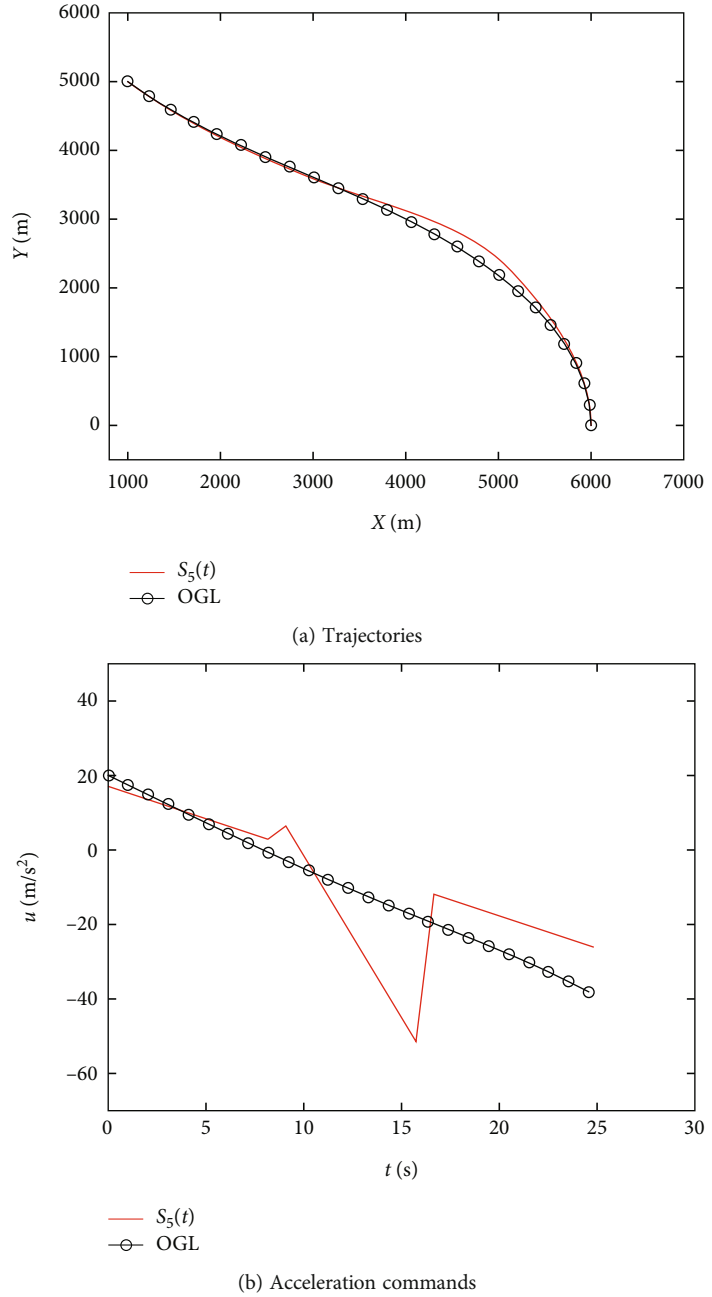

(a) Trajectories

(b) Acceleration commands

FIGURE 17: The comparison results of different weighting functions for $\gamma_m(0) = -45^\circ$, $\gamma_f = -90^\circ$.

($S_3^{(2)}(t)$) or both at the initial and final time ($S_3^{(3)}(t)$) by simply tuning the parameters A_1, B_1, A_2, B_2, w, and t_1. As can be seen, by adopting a piecewise function, the guidance objectives of the Gaussian weighting function and the sinusoidal weighting function can be easily achieved by using a single weighting function $S_3(t)$.

Figure 7 shows the intercept trajectories and guidance commands for $S_3(t)$ with different parameters as listed in Table 3. As shown in Figure 7(a), the proposed guidance law can successfully provide zero miss distance with the desired impact angle for all cases. In Figure 7(b), the guidance command provided by the proposed guidance law is flexibly shaped by simply tuning the designed parameters (i.e., A_1, B_1, A_2, B_2, w, and t_1) of $S_3(t)$. $S_3^{(1)}(t)$ requires small acceleration demands at the final time, which is desired for ensuring the acceleration margin to cope with unanticipated circumstances at the terminal phase. $S_3^{(2)}(t)$ requires small acceleration demands at the initial time, which is desired for alleviating the sensitivity against the initial heading error and is helpful for smooth guidance handover from a midcourse phase to a homing phase. While $S_3^{(3)}(t)$ can simultaneously satisfy both recommended guidance properties of $S_3^{(1)}(t)$ and $S_3^{(3)}(t)$.

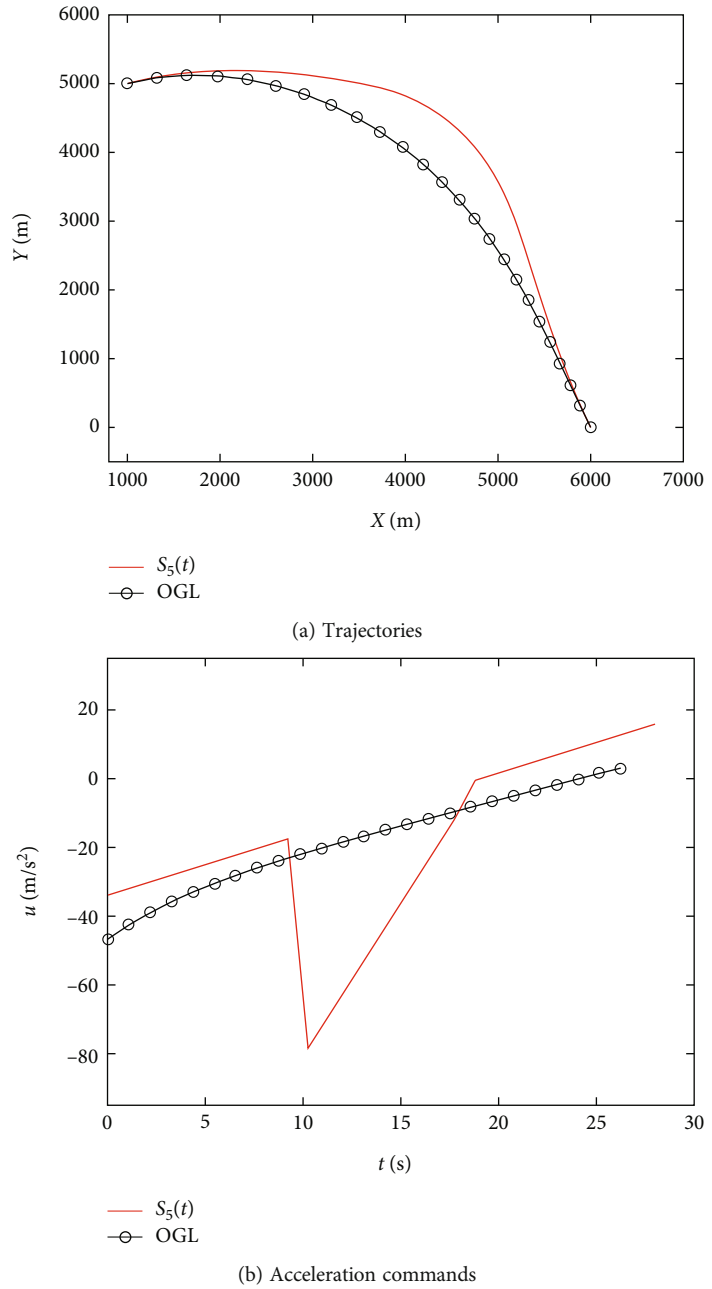

FIGURE 18: The comparison results of different weighting functions for $\gamma_m(0) = 20\circ$, $\gamma_f = -70\circ$.

The intercept trajectories and guidance commands for various initial flight path angles with the desired impact angle as $\gamma_f = -70\circ$ under the weighting functions $S_3^{(1)}(t)$, $S_3^{(2)}(t)$, and $S_3^{(3)}(t)$ are depicted in Figures 8–10. The simulation results show that although the proposed method is derived in the linear system equations, it can be applied to nonlinear engagement cases with a wide range of initial flight path angle sets. In addition, different guidance objectives can be clearly observed with different weighting functions.

The profile of $S_3^{(3)}(t)$ can be further shaped by tuning parameters w and t_1 as illustrated in Figure 11. The corresponding intercept trajectories and guidance commands are illustrated in Figure 12. As can be seen, the duration of the achieved small guidance command at the initial and final time decrease as t_1 decreases, meanwhile the energy expenditure in the middle portion of the engagement decreases. Therefore, for practical guidance applications there is a tradeoff between the energy expenditure and the requirement of small acceleration command in the initial and final phase of the engagement. In addition, through appropriate choices in the design parameters, w and t_1, the missile's trajectory and command profile can be further shaped as desired.

The above simulations show that the proposed method can provide various shapes of the guidance command

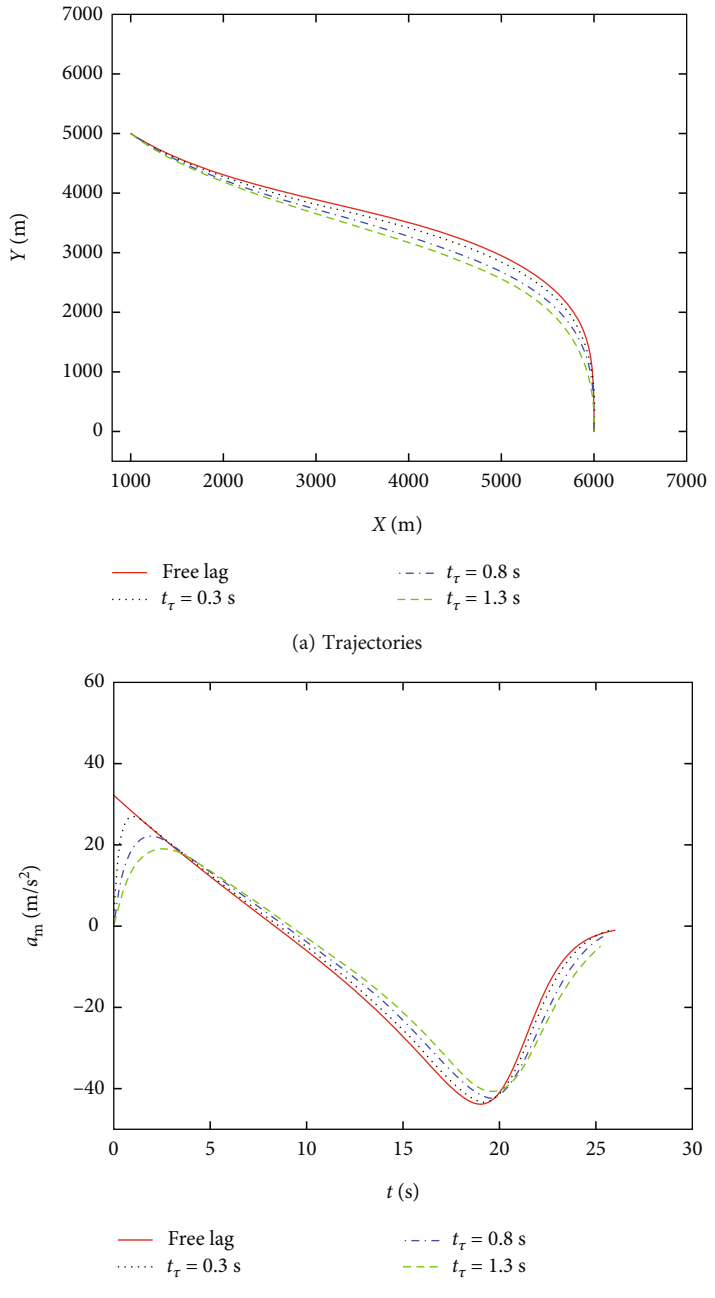

FIGURE 19: Trajectories and commands of the weighting function $\mathbf{S}_3^{(1)}(\mathbf{t})$ for various dynamic lag.

according to appropriate choices of the weighting functions. Most importantly, our method does not need to make any modifications for each new weighting function. This advantage provides more degrees of freedom in the guidance law design with specified guidance objectives. We will show that the proposed guidance law can easily consider nonsmooth or even discontinuous weighting functions in the following cases.

4.2.3. Case 3: Nonsmooth Weighting Function. In this case, we construct a nonsmooth weighting function that consists of a sigmoid function and a Gaussian function as

$$S_4(t) = \begin{cases} \dfrac{2}{1 + e^{-(4.6/w)\left(t - t_f/2\right)}} & 0 \le t \le \dfrac{t_f}{2} \\ \dfrac{1}{e^{\left(t - t_f/2\right)^2 / 2\tau_\sigma^2}} & \dfrac{t_f}{2} < t \le t_f \end{cases}. \tag{42}$$

By selecting the designed parameters as $w = t_f/2.0$ and $\tau_\sigma = t_f/6.0$, the profile of $S_4(t)$ is illustrated in Figure 13. As shown in Figure 13, the weighting function of $S_4(t)$ is expected to provide small acceleration demands at the initial time and the final time, which is similar to $S_2(t)$ and $S_3^{(3)}(t)$.

However, different from $S_2(t)$ and $S_3^{(3)}(t)$, $S_4(t)$ is nonsmooth at $t = t_f/2.0$. This kind of nonsmooth weighting function has not been discussed in previous studies. The main purpose that we design this weighting function is to assess the capacity of the proposed guidance in solving complex weighting functions.

Figures 14 and 15 show the engagement trajectories and guidance commands for the OGL and the proposed guidance law weighted by $S_4(t)$. Although the weighting function is nonsmooth, the proposed guidance can also successfully satisfy the terminal constraints for interception as provided in Figures 14(a) and 15(a). From Figures 14(b) and 15(b), the guidance commands of the proposed guidance law start from small values and also converge to small values as the missile approaches the target. These simulation results are similar to those for $S_2(t)$ and $S_3^{(3)}(t)$, since the profile of $S_4(t)$ is similar to those of $S_2(t)$ and $S_3^{(3)}(t)$. It can be seen from the above results that the proposed guidance is able to handle nonsmooth weighting functions easily, which provides more degrees of freedom in the design of weighting functions.

4.2.4. Case 4: Discontinuous Weighting Function. In this case, we take a discontinuous weighting function as an example to further demonstrate the capacity of the proposed guidance in solving complex weighting functions. The discontinuous weighting function is chosen as

$$S_5(t) = \begin{cases} 0.1 & 0 \le t \le \dfrac{t_f}{3} \\ 1.0 & \dfrac{t_f}{3} < t \le \dfrac{2t_f}{3} \\ 0.1 & \dfrac{2t_f}{3} < t \le t_f \end{cases}. \tag{43}$$

The profile of $S_5(t)$ is shown in Figure 16. $S_5(t)$ is a switching function and is discontinuous at $t = t_f/3.0$ and $t = 2t_f/3.0$. This kind of weighting function has not been considered in previous studies. Simulation results are depicted in Figures 17 and 18. As can be seen, the guidance law can successfully provide zero miss distance with the desired impact angle for all cases. However, due to discontinuities in the weighting function, abrupt command changes are occurred during the engagement. From a practical standpoint, the discontinuous function (43) may not be a good candidate for the design of weighting function. However, this case is mainly used to validate the capacity of the proposed guidance law, and has demonstrated that the proposed guidance can handle the discontinuous weighting function easily. This property makes it possible to design different weighting functions in different engagement phases in order to achieve some specific guidance operational goals, which provides a huge degree of freedom in shaping guidance commands. By using the proposed approach, a new guidance law that allows achieving a specific guidance goal can be easily obtained by devising a proper weighting function (smooth, nonsmooth, or even discontinuous).

4.2.5. Case 5: Extension to the First-Order Lag System. Although the proposed guidance law is derived for the lag-free missile system in Section 3, our approach can be easily extended to handle the guidance problem with dynamic lag effect. Suppose that the missile autopilot model is a first-order delay system:

$$\dot{a}_m(t) = \frac{1}{t_\tau}[a_c(t) - a_m(t)], \tag{44}$$

where $a_c(t)$ and t_τ denote the guidance command and autopilot time delay constant, respectively. Consequently, for the first-order lag missile system, the whole derivation in Section 3 does not require any modification but simply set Equation (5) as $x \triangleq [y \quad \bar{\gamma}_m \quad a_m]^T$, $u \triangleq a_c$, $F \triangleq \begin{bmatrix} 0 & V_m & 0 \\ 0 & 0 & 1/V_m \\ 0 & 0 & -1/t_\tau \end{bmatrix}$, and $G \triangleq \begin{bmatrix} 0 \\ 0 \\ 1/t_\tau \end{bmatrix}$. Then the corresponding matrix $\boldsymbol{S}_f$ is chosen to be $[1 \times 10^4, \ 1 \times 10^4, \ 0]^T$. Figure 19 provides the guidance performance of the proposed guidance law to the first-order lag system for the weighting function $S_3^{(1)}(t)$ with the initial flight path angle as $\gamma_m(0) = -45\circ$ and the desired impact angle as $\gamma_f = -90\circ$. From this figure, we observe that the proposed guidance law can successfully intercept the target for all cases and there is a time delay between the command and response.

5. Conclusions

In this paper, a new computational impact angle control homing guidance law is investigated based on the energy cost weighted by arbitrary functions (smooth, nonsmooth, or even discontinuous), which has the command shaping capacity as desired. By virtue of the Gauss orthogonal collocation method, the optimal control is obtained by solving a set of algebraic equations. The real-time computational capacity of the proposed guidance law is evaluated on a microprocessor. Several types of weighting functions, including smooth, piecewise, nonsmooth, and discontinuous functions, have been tested to evaluate the capacity of the proposed guidance law. Simulation results show that the proposed guidance law can provide various shapes of the guidance command according to appropriate choices of the weighting functions. In addition, profiting from the adoption of a piecewise function, the guidance command shape that provides small acceleration demands at the initial phase, or at the terminal phase, or both at the initial and terminal phases can be easily achieved by using the proposed approach with just one single weighting function. The proposed guidance law is formulated from the generalized optimal control framework and a new guidance law that allows

achieving a specific guidance goal can be easily obtained by devising a proper weighting function (smooth, nonsmooth, or even discontinuous), providing more degrees of freedom in the guidance law design with specified guidance goals.

Data Availability

The data that support the findings of this study are available from the corresponding author upon reasonable request.

Conflicts of Interest

The authors declared no potential conflicts of interest with respect to the research, authorship, and/or publication of this article.

Acknowledgments

This research has been supported by the Natural Science Foundation of Jiangsu Province (No. BK20200498) and the National Natural Science Foundation of China (No. 52202475).

References

[1] H. G. Kim and H. J. Kim, "Field-of-view constrained guidance law for a maneuvering target with impact angle control," *IEEE Transactions on Aerospace and Electronic Systems*, vol. 56, no. 6, pp. 4974–4983, 2020.

[2] P. Pei and J. Wang, "A new optimal guidance law with impact time and angle constraints based on sequential convex programming," *Mathematical Problems in Engineering*, vol. 2021, Article ID 6618351, 15 pages, 2021.

[3] H. Li, J. Wang, S. He, and C. H. Lee, "Nonlinear optimal impact-angle-constrained guidance with large initial heading error," *Journal of Guidance, Control, and Dynamics*, vol. 44, no. 9, pp. 1663–1676, 2021.

[4] Y. I. Lee, C. K. Ryoo, and E. Kim, "Optimal guidance with constraints on impact angle and terminal acceleration," in *AIAA Guidance, Navigation, and Control Conference and Exhibit*, Austin, Texas, 2003.

[5] V. Shaferman and T. Shima, "Linear quadratic guidance laws for imposing a terminal intercept angle," *Journal of Guidance, Control, and Dynamics*, vol. 31, no. 5, pp. 1400–1412, 2008.

[6] S. Xiong, W. Wang, X. Liu, S. Wang, and Z. Chen, "Guidance law against maneuvering targets with intercept angle constraint," *ISA Transactions*, vol. 53, no. 4, pp. 1332–1342, 2014.

[7] W. Yu, W. Chen, L. Yang, X. Liu, and H. Zhou, "Optimal terminal guidance for exoatmospheric interception," *Chinese Journal of Aeronautics*, vol. 29, no. 4, pp. 1052–1064, 2016.

[8] F. He, W. Chen, and Y. Bao, "Novel particle swarm optimization guidance for hypersonic target interception with impact angle constraint," *International Journal of Aerospace Engineering*, vol. 2022, Article ID 7615644, 10 pages, 2022.

[9] Z. Hou, Y. Yang, L. Liu, and Y. Wang, "Terminal sliding mode control based impact time and angle constrained guidance," *Aerospace Science and Technology*, vol. 93, article 105142, 2019.

[10] J. Guo, Y. Li, and J. Zhou, "Qualitative indicator-based guidance scheme for bank-to-turn missiles against couplings and maneuvering targets," *Aerospace Science and Technology*, vol. 106, article 106196, 2020.

[11] D. Cho and S. H. Kim, "Direct impact angle control guidance for passive homing missiles," *Proceedings of the Institution of Mechanical Engineers, Part G: Journal of Aerospace Engineering*, vol. 234, no. 15, pp. 2139–2152, 2020.

[12] Y. Tan, W. Jing, C. Gao, and R. An, "Adaptive improved super-twisting integral sliding mode guidance law against maneuvering target with terminal angle constraint," *Aerospace Science and Technology*, vol. 129, article 107820, 2022.

[13] X. Yan, J. Zhu, M. Kuang, and X. Yuan, "A computational-geometry-based 3-dimensional guidance law to control impact time and angle," *Aerospace Science and Technology*, vol. 98, article 105672, 2020.

[14] B. Liu, M. Hou, Y. Yu, and Z. Wu, "Three-dimensional impact angle control guidance with field-of-view constraint," *Aerospace Science and Technology*, vol. 105, article 106014, 2020.

[15] Q. Hu, T. Han, and M. Xin, "Analytical solution for nonlinear three-dimensional guidance with impact angle and field-of-view constraints," *IEEE Transactions on Industrial Electronics*, vol. 68, no. 4, pp. 3423–3433, 2021.

[16] H. Yu, K. Dai, H. Li et al., "Three-dimensional adaptive fixed-time cooperative guidance law with impact time and angle constraints," *Aerospace Science and Technology*, vol. 123, article 107450, 2022.

[17] D. Zhou, C. Mu, and T. Shen, "Robust guidance law with L_2 gain performance," *Transactions of the Japan Society for Aeronautical and Space Sciences*, vol. 44, no. 144, pp. 82–88, 2001.

[18] M. Kim and K. V. Grider, "Terminal guidance for impact attitude angle constrained flight trajectories," *IEEE Transactions on Aerospace and Electronic Systems*, vol. AES-9, no. 6, pp. 852–859, 1973.

[19] C. K. Ryoo, H. Cho, and M. J. Tahk, "Optimal guidance laws with terminal impact angle constraint," *Journal of Guidance, Control, and Dynamics*, vol. 28, no. 4, pp. 724–732, 2005.

[20] T. L. Song, S. J. Shin, and H. Cho, "Impact angle control for planar engagements," *IEEE Transactions on Aerospace and Electronic Systems*, vol. 35, no. 4, pp. 1439–1444, 1999.

[21] X. Chen and J. Wang, "Optimal control based guidance law to control both impact time and impact angle," *Aerospace Science and Technology*, vol. 84, pp. 454–463, 2019.

[22] J. Zhu, D. Su, Y. Xie, and H. Sun, "Impact time and angle control guidance independent of time-to-go prediction," *Aerospace Science and Technology*, vol. 86, pp. 818–825, 2019.

[23] E. Ohlmeyer and C. Phillips, "Generalized vector explicit guidance," *Journal of Guidance, Control, and Dynamics*, vol. 29, no. 2, pp. 261–268, 2006.

[24] C. K. Ryoo, H. Cho, and M. J. Tahk, "Time-to-go weighted optimal guidance with impact angle constraints," *IEEE Transactions on Control Systems Technology*, vol. 14, no. 3, pp. 483–492, 2006.

[25] N. Cho, Y. Kim, and C. H. Lee, "Schwarz inequality method for weighted minimum effort terminal control of multidimensional systems," *Journal of Guidance, Control, and Dynamics*, vol. 43, no. 10, pp. 1893–1903, 2020.

[26] J. Ben-Asher, N. Farber, and S. Levinson, "New proportional navigation law for ground-to-air systems," *Journal of Guidance, Control, and Dynamics*, vol. 26, no. 5, pp. 822–825, 2003.

[27] M. Y. Ryu, C. H. Lee, and M. J. Tahk, "Command shaping optimal guidance laws against high-speed incoming targets," *Journal of Guidance, Control, and Dynamics*, vol. 38, no. 10, pp. 2025–2033, 2015.

[28] J. I. Lee, I. S. Jeon, and C. H. Lee, "Command-shaping guidance law based on a Gaussian weighting function," *IEEE Transactions on Aerospace and Electronic Systems*, vol. 50, no. 1, pp. 772–777, 2014.

[29] C. H. Lee, J. I. Lee, and M. J. Tahk, "Sinusoidal function weighted optimal guidance laws," *Proceedings of the Institution of Mechanical Engineers, Part G: Journal of Aerospace Engineering*, vol. 229, no. 3, pp. 534–542, 2015.

[30] S. Xiong, M. Wei, M. Zhao, H. Xiong, W. Wang, and B. Zhou, "Hyperbolic tangent function weighted optimal intercept angle guidance law," *Aerospace Science and Technology*, vol. 78, pp. 604–619, 2018.

[31] C. H. Lee and J. I. Lee, "Generalized formulation of weighted optimal guidance laws with impact angle constraint," *IEEE Transactions on Aerospace and Electronic Systems*, vol. 49, no. 2, pp. 1317–1322, 2013.

[32] C. H. Lee and M. Y. Ryu, "Practical generalized optimal guidance law with impact angle constraint," *Proceedings of the Institution of Mechanical Engineers, Part G: Journal of Aerospace Engineering*, vol. 233, no. 10, pp. 3790–3809, 2019.

[33] C. Li, J. Wang, S. He, and C. H. Lee, "Collision-geometry-based generalized optimal impact angle guidance for various missile and target motions," *Aerospace Science and Technology*, vol. 106, article 106204, 2020.

[34] P. Davis and P. Rabinowitz, "Methods of numerical integration," Academic Press, New York, NY, USA, 1984.

[35] D. A. Benson, "A Gauss pseudospectral transcription for optimal control," Department of Aeronautics and Astronautics, MIT, USA, 2004.